Electrochemical Characterization of Electrodeposited Copper Catalyst for CCU

Corentin Penot , Kranthi Kumar Maniam , Shiladitya Paul *

Posted Date: 28 March 2024

doi: 10.20944/preprints202403.1749.v1

Keywords: Electrodeposition; Copper; Electrochemical CO2 reduction; Corrosion; Amine CO2 capture; Carbon capture and utilization

Article

Electrochemical Characterization of Electrodeposited Copper Catalyst for CCU

Corentin Penot [1], Kranthi Kumar Maniam [1] and Shiladitya Paul [1,2,*]

[1] Materials Innovation Centre, School of Engineering, University of Leicester, Leicester, LE1 7RH, UK; cp473@leicester.ac.uk (C.P.); km508@leicester.ac.uk (K.K.M.)
[2] Materials Performance and Integrity Technology Group, TWI, Cambridge, CB21 6AL, UK
* Correspondence: shiladitya.paul@twi.co.uk

Abstract: This study explores the stability of electrodeposited copper catalysts utilized in electrochemical CO_2 reduction (ECR) across various amine media. The focus is on understanding the influence of different amine types, corrosion ramifications, and the efficacy of pulse ECR methodologies. Employing a suite of electrochemical techniques including potentiodynamic polarization, linear resistance polarization, cyclic voltammetry, and chronopotentiometry, the investigation reveals useful insights. The findings show that among the tested amines, CO_2-rich monoethanolamine (MEA) exhibits the highest corrosion rate. However, in most cases the rates remain within tolerable limits for ECR operations. Primary amines, notably monoethanolamine (MEA), show enhanced compatibility with ECR processes, attributable to their resistance against carbonate salt precipitation and sustained stability in potential over extended durations. Conversely, tertiary amines such as methyldiethanolamine (MDEA) present challenges due to the formation of carbonate salts during ECR, impeding their effective utilization. The study highlights the effectiveness of pulse ECR strategies in stabilizing ECR. A noticeable shift in cathodic potential and reduced deposit formation on the catalyst surface through periodic oxidation underscores the efficacy of such strategies. These findings offer insights for optimizing ECR in amine media, thereby providing promising pathways for advancements in CO_2 emission reduction technologies.

Keywords: electrodeposition; copper; electrochemical CO_2 reduction; corrosion; amine CO_2 capture; carbon capture and utilization

1. Introduction

Mitigating climate change necessitates urgent action to reduce CO_2 emissions. Achieving net zero CO_2 emissions by 2050 is critical to limit the temperature rise to below 1.5 °C, in line with the Paris Agreement (COP21) objectives [1]. To address this challenge, the development of CO_2 capture technologies is a priority. Currently, the most advanced industrial technology employs aqueous amine solutions such as monoethanolamine (MEA), methyldiethanolamine (MDEA) and 2-amino-2-methylpropanol (AMP) for CO_2 capture. This process entails direct CO_2 capture from flue gas stream and its subsequent release by heating the CO_2-rich amine capture media in a desorber unit at approximately 120°C [2]. The regenerated amine then re-enters the capture cycle. However, the regeneration step, accounting for up to 30% of the total plant energy output, is highly energy-intensive [3]. This issue may be overcome by regenerating the CO_2-rich amine media using electrochemical CO_2 reduction (ECR) instead. This approach features the direct transformation of amine-CO_2 adducts, such as carbamates, into valuable chemicals [4]. The seamless integration of amine-based CO_2 capture and ECR demonstrates good synergy. This approach not only bypasses challenges related to CO_2 transportation and storage but also eradicates the necessity for regenerating capture media through the thermal release of molecular CO_2 [5].

ECR is an emerging field, evolving independently from carbon capture technologies. It presents significant synergies with other climate change challenges, notably in storing surplus renewable

 doi:10.20944/preprints202403.1749.v1

electricity. ECR converts excess electricity into valuable, energy-dense products like CO, ethylene, ethanol etc. The output product spectrum depends on the applied potential, catalyst, and cell configuration [6]. Copper is unique in promoting valuable C_{2+} products like ethylene and is therefore widely employed as a catalyst [7]. Achieving economic viability in ECR hinges on meeting specific performance benchmarks, including current density, Faradaic efficiency (FE), energy efficiency (EE), and stability [8]. Recent research has made significant strides in improving current density, FE, and EE. Notably, current densities over 1 A cm^{-2} with 45% EE for ethylene production using copper gas diffusion electrodes (GDEs) have been achieved [9]. Ongoing efforts aim to enhance selectivity toward C_{2+} products through advanced copper-based catalysts [10–12]. However, stability improvements remain a less explored yet critical aspect for viable ECR. Copper catalysts often undergo rapid degradation due to surface reconstruction, poisoning, and carbonate salt precipitation [13]. Studies by Huang et al. [14] and Simon et al. [15] show that cathodic potential drives copper catalyst surface reconstruction and refaceting. This process results in decreased selectivity towards C_{2+} products, undermining long-term catalyst performance [16–19]. Another challenge for stable ECR is carbonate salt precipitation on the catalyst surface [20–22]. The local high pH near the electrode, due to HO^- production in the CO_2 reduction reaction, facilitates carbonate salt formation through reaction with cations.

Recent advancements in electrochemical CO_2 reduction (ECR) have highlighted pulse ECR as a method to enhance long-term process performance [23]. Pulse ECR involves interspersing short anodic segments with longer cathodic ones to regenerate the catalytic properties of copper by inducing oxidation. Obasanjo et al. [24] demonstrated that this oxidation process reactivates C_{2+} active sites by removing Cu-OH, which gradually deactivates the catalyst. Xu et al. [21] successfully employed pulse ECR to sustain high Faradaic efficiency (FE) towards C2+ products over 36 hours, observing that Cu(I) oxide formation is advantageous for C2+ product formation and can be regenerated through anodic pulsing. Similarly, Zhang et al. [25] found that a combination of Cu(0) and Cu(I) states favours C_{2+} products, maintaining a high FE (70%) towards ethylene across 145 hours of operation using pulse ECR. Complementary studies have shown that appropriate pulse strategies can enhance and modulate long-term selectivity of ECR [26,27], while also mitigating catalyst poisoning [28] and carbamate salt formation [21,29].

Research on ECR, including pulse ECR has largely focused on using aqueous carbonate (KOH + CO_2) or bicarbonate ($KHCO_3$ + CO_2) solutions. Increasing efforts are now directed towards integrating ECR with amine-based CO_2 capture. Various studies have reported carbamate reduction to CO [30], formate [31,32], or both [33] using metal electrodes like copper [30,32]. However, the long-term stability of these catalytic properties remains unexplored. Additionally, the impact of amines on copper corrosion is a growing concern [5], with some studies suggesting significant copper degradation in MEA under halted cathodic potential [34], which necessitates further investigation.

In this study, we explore the electrochemical and corrosion properties of electrodeposited copper in amine-based electrolytes under CO_2-lean and -rich conditions. We also examine the stability of the copper catalyst under cathodic polarization relevant to CO_2 reduction. Different pulse polarization strategies are tested to assess the impact of pulse ECR in amine media.

2. Materials and Methods

2.1. Specimen Preparation and Characterisation

Copper was electrodeposited onto a copper substrate using a method detailed in the Supplementary Information. Following electrodeposition, specimens were selectively masked with resin provided by Belzona Ltd. (UK, reference 1395) resin, resulting in an exposed surface area of approximately 1 cm^2 for each specimen. To characterize the surfaces of these specimens, an optical microscope BX41M-LED from Olympus (JPN) and a Sigma 1455EP scanning electron microscope (SEM) from Ziess (GER) were employed.

 doi:10.20944/preprints202403.1749.v1

2.2. Amine Media

Four amine-based media, commonly employed for CO_2 capture, were evaluated:

- 30 wt.% Monoethanolamine (MEA), CAS: 141-43-5, a primary amine extensively utilized for CO_2 capture [2].
- 37 wt.% Methyldiethanolamine (MDEA) CAS: 105-59-9, a tertiary amine
- 30 wt.% MDEA + 21 wt.% piperazine (PZ), CAS: 110-85-0, generally used to improve capture kinetics [35].
- 30 wt.% 2-Amino-2-methyl-1-propanol (AMP), CAS: 124-68-5, a sterically hindered primary amine known for its elevated CO_2 absorption capacity [36].

The anolyte for these experiments was 0.5 M potassium chloride (KCl) solution. Additionally, 0.5 M KCl was incorporated into the amine solutions to enhance their electrical conductivity. All chemicals used in solution preparation were of laboratory grade and supplied by Merck Life Science UK Ltd. (UK).

In subsequent discussions and analyses, these solutions are referred to as MEA, MDEA, MDEA/PZ, and AMP for simplicity.

2.2. Electrochemical Tests

Electrochemical experiments were conducted using a Biologic (FR) VMP-300 potentiostat and a 100 mL H-cell sourced from Dek research (US). The experimental setup featured anodic and cathodic compartments, separated by a Nafion 117 proton exchange membrane (Dupont, US) which underwent appropriate activation before use. The reference electrode comprised an Ag/AgCl in 3.5 M KCl, positioned in a Luggin capillary filled with 3.5 M KCl to isolate it from the amine electrolyte. The capillary's tip was situated 5 mm from the specimen. A platinum mesh served as the counter electrode. The cell design included gas inlet/outlet provisions for purging the solution with CO_2. Each specimen was kept at -0.5 V relative to the Open Circuit Potential (OCP) for 5 minutes before testing to remove the air-formed oxide layer.

Linear polarization resistance (LPR), potentiodynamic polarization (PDP), and cyclic voltammetry (CV) tests were performed after recording and stabilizing the OCP for 1 h. To ensure reproducibility, each measurement was conducted in triplicate. For brevity, Figure 2 displays a single representative polarization scheme per experimental condition, with the full dataset accessible in Figure 1 of the Supplementary Information document. LPR results are presented in Supplementary Information Figure 2. The test solutions were maintained at ambient laboratory conditions (20 ± 2 °C) and could be CO_2-purged as required. LPR tests utilized a potential offset of ±20 mV relative to OCP at a scan rate of 0.125 mV s^{-1}. PDP involved potential sweeping from -0.2 V to +0.2 V versus OCP at a rate of 10 mV min^{-1}. CV scans were conducted at 20 mV s^{-1} scan rate, reversing the scan when the current density reached |10| mA cm^{-2} for both cathodic and anodic polarizations.

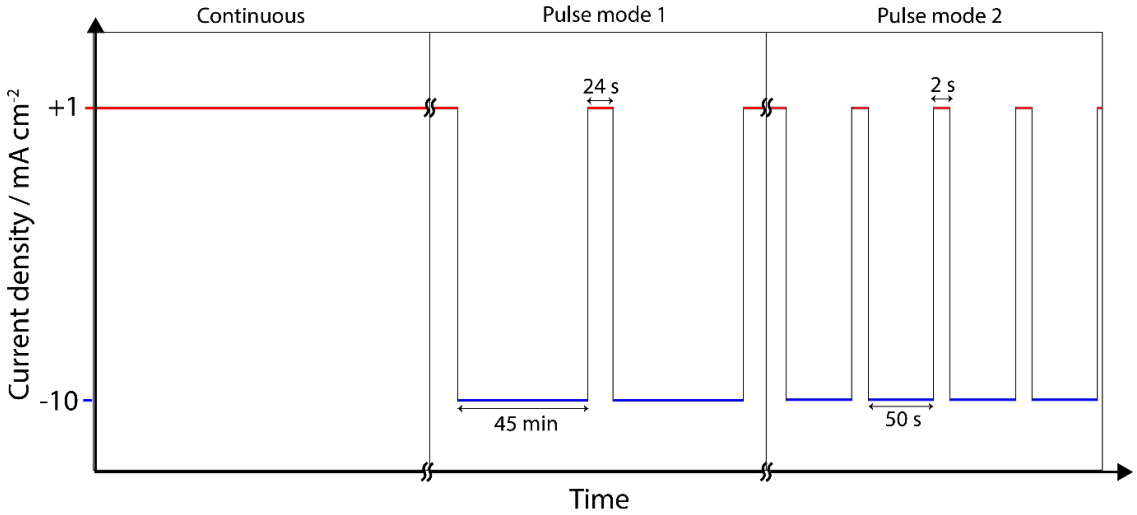

 doi:10.20944/preprints202403.1749.v1

Figure 1. Three modes of chronopotentiometry: (1) continuous polarization at -10 mA cm^{-2} for 60 h; (2) pulse mode 1, 45 min at -10 mA cm^{-2} for 24 s at +1 mA cm^{-2} repeated 80 times; (3) pulse mode 2, 50 s at -10 mA cm^{-2} for 2 s at +1 mA cm^{-2} repeated 4320 times.

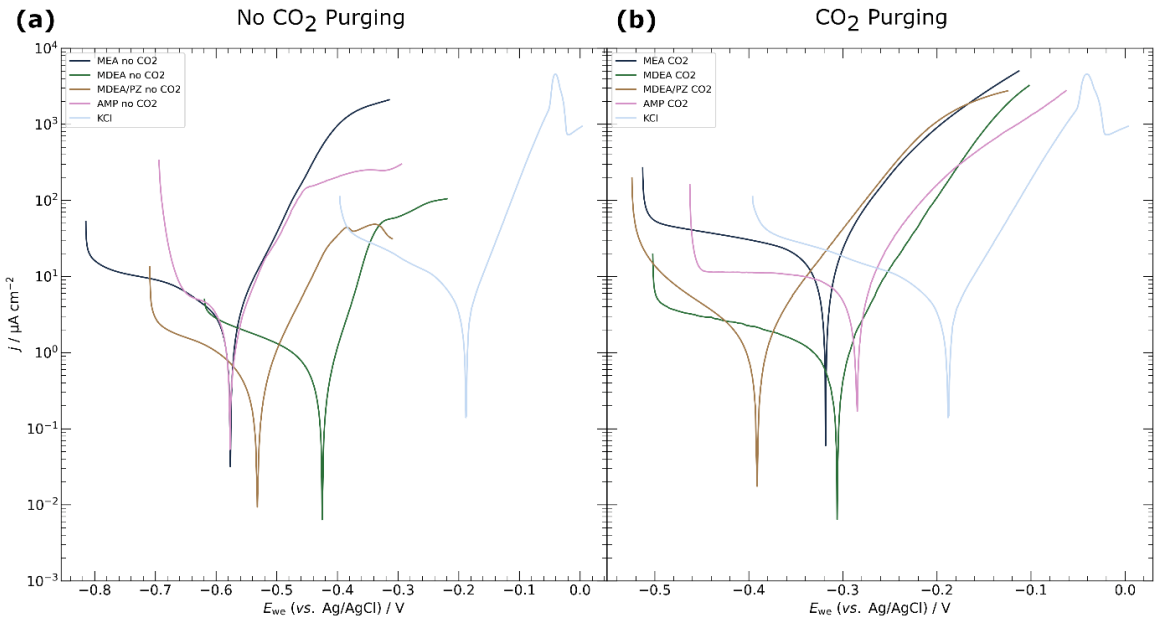

Figure 2. Potentiodynamic polarization of copper specimens in the different amine-based capture media. **(a)** without CO_2 and **(b)** with CO_2 purging. Scan rate 10 mV min^{-1}.

Chronopotentiometry experiments were designed to simulate 60 hours of ECR. Three strategies, that included alternating anodic and cathodic segments, were implemented as detailed in **Figure 1**. Anodic segments were conducted at +1 mA cm^{-2}, while cathodic segments operated at -10 mA cm^{-2}, cumulatively totalling 60 hours for cathodic segments. Pulse mode 1 consisted of a 24-second anodic segment every 45 minutes, and pulse mode 2 involved a 2-second anodic segment every 50 seconds.

Electrochemical tests underwent iR compensation utilizing the potentiostat's built-in feature, which is based on high-frequency impedance measurements. The average cell resistances determined for each media are systematically tabulated in Supplementary Information Table S1.

3. Results

3.1. Electrochemical Characterisation of Electrodeposited Copper in Amine Media

Potentiodynamic polarizations were performed in triplicate under both CO_2-free and CO_2-purged conditions across various amine media. For each scenario, a representative curve was selected for display in **Figure 2**, with the comprehensive set of polarization data provided in the Supplementary Information Figure 1. The Tafel extrapolation method was employed to estimate the corrosion current density (j_{corr}) [37]. The average j_{corr} values, together with the corresponding corrosion potentials (E_{corr}), are compiled in **Table 1**.

Table 1. Average corrosion potential (E_{corr}), corrosion current density (j_{corr}) and polarization resistance (R_p) for electrodeposited copper specimens in different amine media.

Media	CO_2	E_{corr} / V	j_{corr} / μA cm^{-2}	R_p / kΩ cm^2
MEA	no	-0.58 ± 0.01	2.4 ± 0.1	3.8 ± 0.7
	yes	-0.29 ± 0.02	14.1 ± 6.9	0.7 ± 0.2
MDEA	no	-0.42 ± 0.01	0.3 ± 0.1	19.0 ± 4.4
	yes	-0.33 ± 0.03	1.0 ± 0.1	10.4 ± 0.5

 doi:10.20944/preprints202403.1749.v1

MDEA/PZ	no	-0.53 ± 0.01	0.4 ± 0.1	18.3 ± 6.3
	yes	-0.39 ± 0.01	0.9 ± 0.6	12.6 ± 11.3
AMP	no	-0.57 ± 0.01	1.5 ± 0.3	5.6 ± 1.1
	yes	-0.29 ± 0.02	7.7 ± 1.3	1.0 ± 0.6
KCl	no	-0.20 ± 0.03	2.4 ± 0.6	3.7 ± 1.1

In environments devoid of CO_2, j_{corr} values for all amines were lower compared to 0.5 M KCl. Specifically, MDEA and MDEA/PZ exhibited reduced j_{corr} values relative to MEA and AMP, with the latter two showing j_{corr} values comparable to KCl. Upon introducing CO_2, a notable shift in E_{corr} towards more anodic potentials occurred for all amines, attributable to the dissolution of CO_2 and the formation of carbonate/bicarbonate species. Concurrently, the introduction of CO_2 resulted in an increase in j_{corr} across all amines. The relative order of j_{corr} values remained consistent with the CO_2-free cases: MEA and AMP exhibited higher j_{corr}, exceeding that of KCl, while MDEA and MDEA/PZ maintained significantly lower values. Polarization resistances (R_p) data, derived from LPR measurements, were consistent with j_{corr}. Lower R_p values, indicative of higher corrosion rates, were observed for CO_2-loaded MEA and AMP, whereas CO_2-free MDEA and MDEA/PZ demonstrated higher resistances.

CV scans, presented in **Figure 3**, reveal distinct electrochemical behaviours of copper in various amine media. For comparative purposes, CV experiments were also conducted in 0.5 M KCl. In CO_2-lean amine media, two oxidation peaks (A and B) were identified and two reduction peaks (C and D). It is well established that copper oxidizes to form either Cu(I) or Cu(II) [38]. During the anodic sweep, the initial peak (A) is attributed to the formation of Cu(I), while the subsequent peak (B) corresponds to Cu(II) oxidation, both manifesting as copper oxides/hydroxides and their hydrated forms. The oxidation current increase beyond peak B signifies the formation of soluble copper ions such as CuO_2^-, until the onset of oxygen evolution at more anodic potentials. The onset potential for peak A remains relatively consistent across all CO_2-free amine media, approximately at 0.45 V. However, the onset for peak B varies significantly, indicating a more complex oxidation mechanism, in line with previous findings in KOH solutions [39]. In MEA, the lowest onset potential leads to the overlapping of peaks A and B. In contrast, MDEA, MDEA/PZ, and AMP exhibit distinct B peaks at more anodic potentials, at -0.27 V, -0.15 V, and -0.27 V respectively. Peaks C and D are associated with the reduction of Cu(I) and Cu(II) species, while the highest cathodic current surge is attributed to the hydrogen evolution reaction (HER).

 doi:10.20944/preprints202403.1749.v1

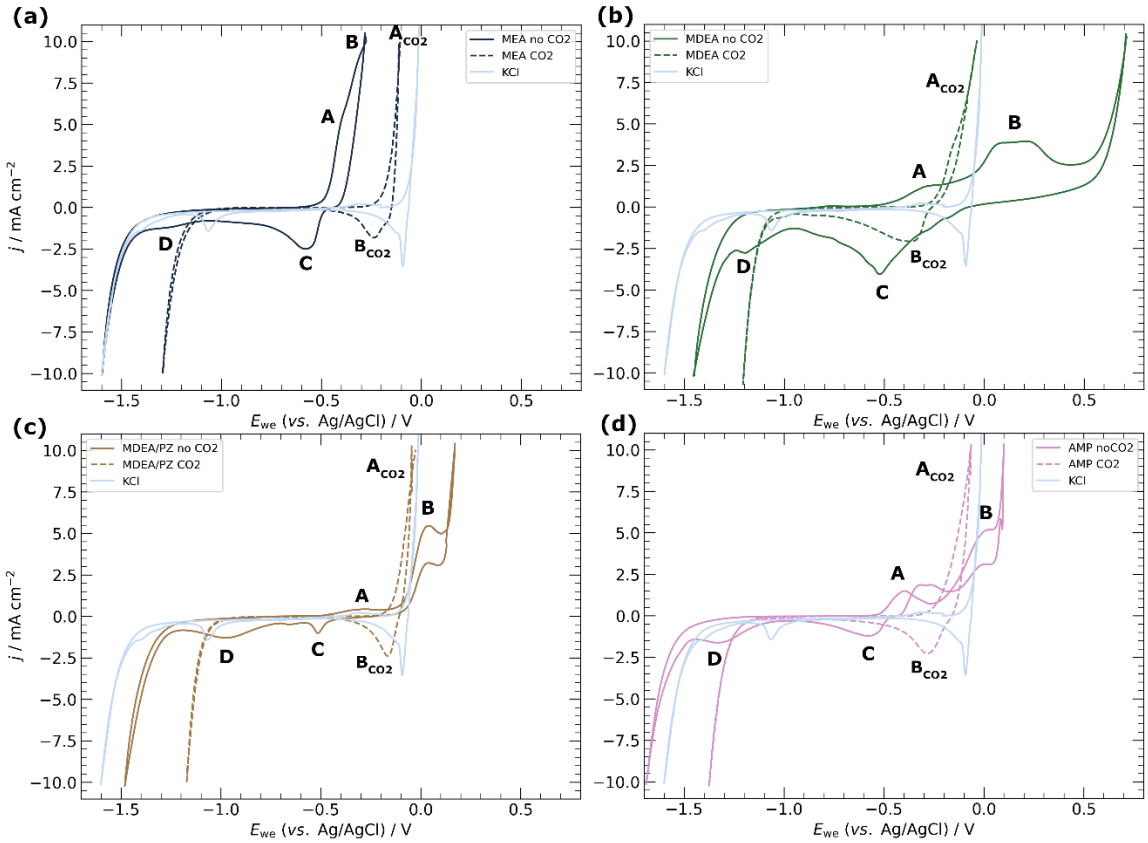

Figure 3. Cyclic voltammetry of electrodeposited copper specimens in different amine-based capture media under CO_2-lean and CO_2-rich conditions: **(a)** MEA, **(b)** MDEA, **(c)** MDEA/PZ, **(d)** AMP. Scan rate 20 mV s^{-1}.

In CO_2-rich amine media, only two peaks, labelled A_{CO2} and B_{CO2}, are evident. Peak A_{CO2} could represent the overlap of peaks A and B, indicating the concurrent formation of both Cu(I) and Cu(II) species, or it might signify the exclusive formation of Cu(II) species. The former scenario seems more probable, as the overlapping of peaks A and B has been previously reported in high pH conditions [39], likely influenced by CO_2 purging. The onset oxidation potentials in various amines are closer in the CO_2-rich environment, recorded at -0.21 V, -0.27 V, -0.17 V, and -0.25 V for MEA, MDEA, MDEA-PZ, and AMP, respectively. This observation underscores the significant impact of the presence of CO_2 on copper oxidation and supports previous PDP and LPR data. Copper oxidizes more readily in CO_2-rich media, as evidenced by a steeper increase in oxidation current at more cathodic potentials, except for MEA, which exhibits a slightly higher oxidation onset potential in CO_2-rich conditions. In CO_2-rich amines, the most anodic current is either due to HER or the CO_2 reduction reaction (CO_2RR),and is shifted towards more anodic potentials. This shift suggests that CO_2RR may have a more anodic onset potential than HER, leading to an observable increase in current density on the CV scan for CO_2-purged media.

3.1. Chronopotentiometry

Specimens underwent cathodic polarization for a cumulative duration of 60 hours, employing varied pulse strategies. These strategies encompassed continuous cathodic polarization, pulse mode 1, and pulse mode 2, detailed in **Figure 1**. The potential as a function of time was closely monitored, with the corresponding cathodic chronopotentiometry results displayed in **Figure 4**. Anodic chronopotentiometry results are similarly detailed in **Figure 5**.

 doi:10.20944/preprints202403.1749.v1

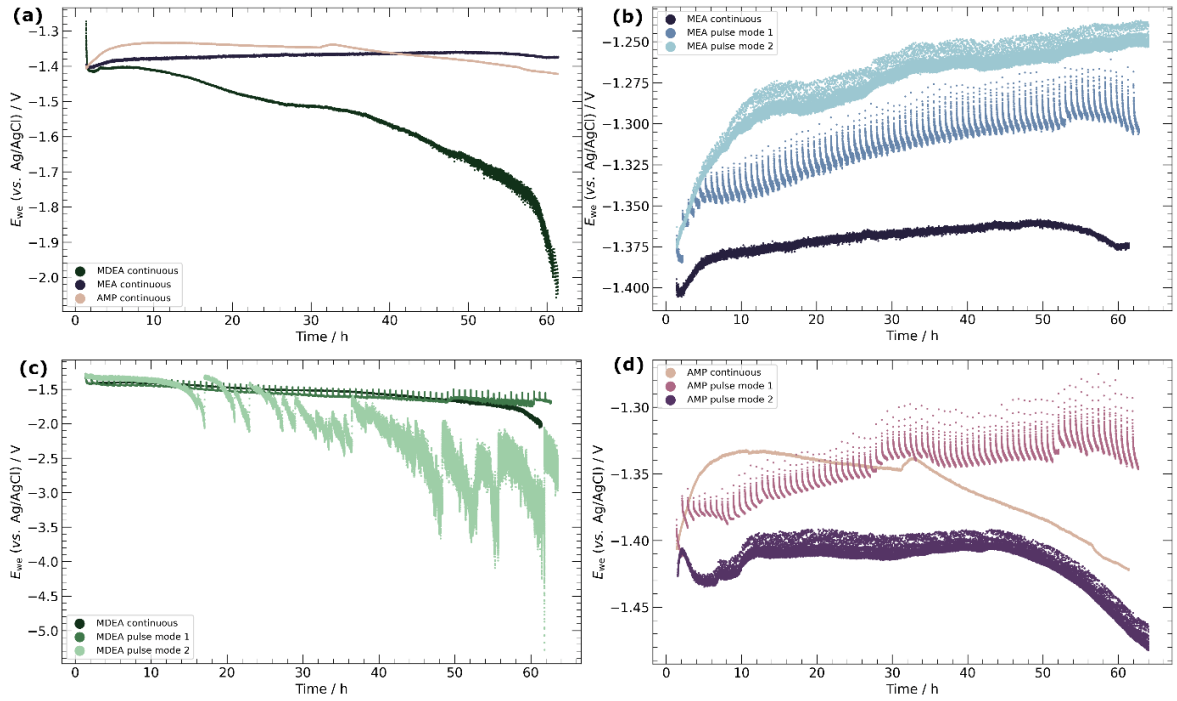

Figure 4. Cathodic chronopotentiometry of electrodeposited copper specimen in 30 wt.% MEA, 5 m MDEA and 30 wt.% AMP solutions purged with CO_2. **(a)** continuous cathodic polarization; **(b)**, **(c)**, **(d)** continuous and pulse mode 1 and 2 in MEA, MDEA and AMP, respectively. Target current density was -10 mA cm^{-2}.

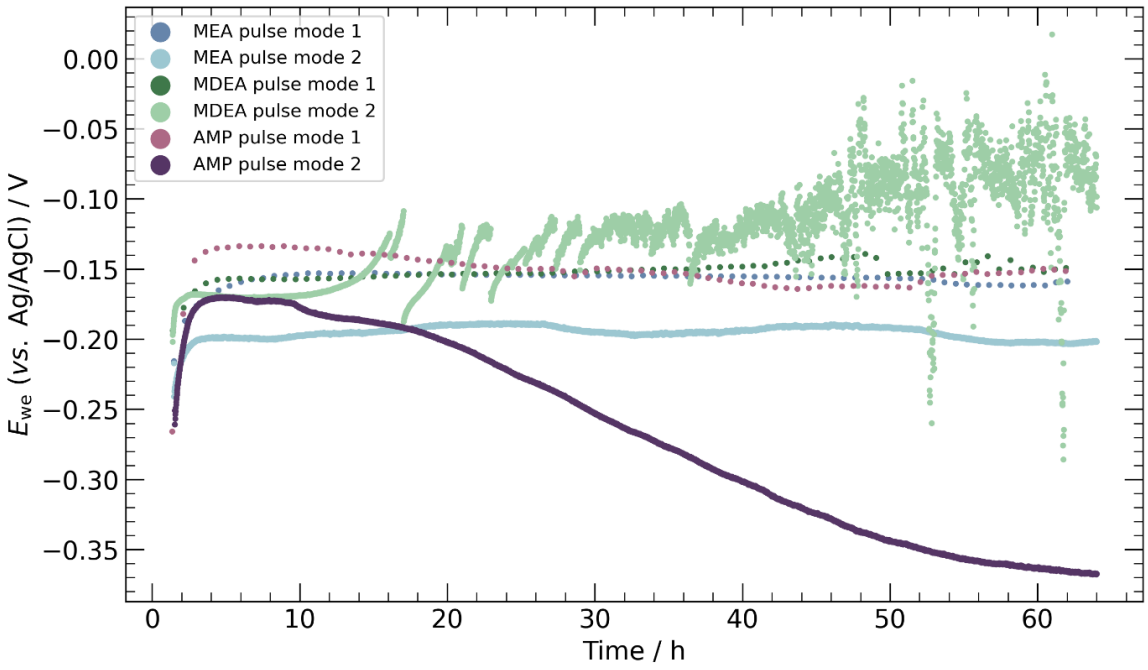

Figure 5. Anodic segments from chronopotentiometry of electrodeposited copper specimen in 30 wt.% MEA, 5 m MDEA and 30 wt.% AMP solutions purged with CO_2. Target current density was +1 mA cm^{-2}. Only the last data point of each cycle is represented for clarity.

Chronopotentiometry results for continuous cathodic polarization over 60 hours in MEA, MDEA, and AMP are illustrated in **Figure 4**a. In MDEA/PZ, this experiment was hindered by the formation of carbonate salts, which obstructed the CO_2 gas inlet after only 2-3 hours. Similar

 doi:10.20944/preprints202403.1749.v1

carbonate salt precipitation was observed in MDEA, leading to an unstable cathodic potential that progressively shifted towards more cathodic values, as depicted in **Figure 4**a. In contrast, the potentials in AMP demonstrated greater stability, albeit with a slight decrease over time. Notably, MEA exhibited the most stable potential, concluding the experiment at a potential 20 mV higher than the initial value.

The influence of pulse strategies on potential evolution for the various amine solutions is highlighted in **Figure 4**b–d. Employing a lower frequency pulse strategy (pulse mode 1) consistently improved potential stability across all amine solutions. In the case of MDEA, this strategy resulted in a stable potential decrease beyond 55 hours, contrasting with the trend observed under continuous polarization. For MEA and AMP, pulse mode 1 induced a gradual electropositive shift in potential, reaching increments of +70 mV and +65 mV from their initial values, respectively. The adoption of a higher frequency of anodic segments (pulse mode 2) demonstrated diverse outcomes. In MEA, pulse mode 2 more significantly improved potential stability compared to pulse mode 1, achieving an increase of +125 mV compared to the initial value. In contrast, for AMP, the potential under pulse mode 2 initially remained stable but began to decline after 45 hours, aligning more closely with the behaviour observed under continuous polarization. For MDEA, the potential during pulse mode 2 rapidly deteriorated and became extremely unstable upon the onset of carbonate salt precipitation.

Anodic chronopotentiometry results for the various pulse strategies are shown in **Figure 5**. Three distinct behaviours emerged: stable, erratic, and decreasing. A stable potential was noted in all specimens subjected to pulse mode 1, as well as in MEA under pulse mode 2. The potential required to reach a current density of +1 mA cm^{-2} hovered around -0.15 V for pulse mode 1 and -0.2 V for pulse mode 2 in MEA. This variance is attributed to surface charging/discharging phenomena, necessitating more anodic potentials to offset the declining discharging current with an elevated Faradaic oxidation current for longer anodic durations. Since pulse mode 2 features shorter durations, the proportion of Faradaic current is reduced, hence less anodic potentials are sufficient to sustain the target current density.

In the case of MDEA and AMP under pulse mode 2, the anodic potential exhibited instability, albeit with markedly different behaviours. In MDEA using pulse mode 2, an erratic potential was observed beyond 15 hours, likely caused by the intermittent formation and detachment of carbonate salts on the catalyst surface. In contrast, AMP during pulse mode 2 exhibited a continuous cathodic shift in anodic potential over time.

The post-chronopotentiometry visual appearance of copper catalysts exhibits marked variations contingent on the polarization mode, as illustrated in Figure 6. Continuously polarized specimens display darker surfaces, whereas those subjected to pulse modes generally manifest ‘cleaner’ copper surfaces, with the exception of AMP under pulse mode 2. When correlating the visual observations of the catalysts post-chronopotentiometry with the anodic potential data from **Figure 5**, it becomes evident that periodic oxidation facilitated by pulse modes effectively mitigates the formation of dark deposits. The pronounced dark deposit observed in AMP under pulse mode 2 indicates inadequate oxidation of the copper catalyst. Indeed, several factors can contribute to an cathodic shift in potential when maintaining a target anodic current density, such as a reduction in active surface area, a shift in oxidation onset potential, or an increased charging of the interface reducing the proportion of Faradaic currents required to achieve the target. The observed potential diminution for AMP pulse mode 2 is presumably attributed to the latter, as post-test surface characterization revealed a dark deposit akin to that observed following continuous polarization, as shown in **Figure 6**. This suggests that the intended oxidation of copper was not effectively achieved, pointing to surface charging as the underlying cause for the diminished oxidation. Under these specific test conditions, an anodic duration of 2 seconds proved insufficient for achieving copper oxidation in CO_2-rich AMP. These findings underscore the importance of cyclic copper oxidation in preventing the formation of such dark deposits.

 doi:10.20944/preprints202403.1749.v1

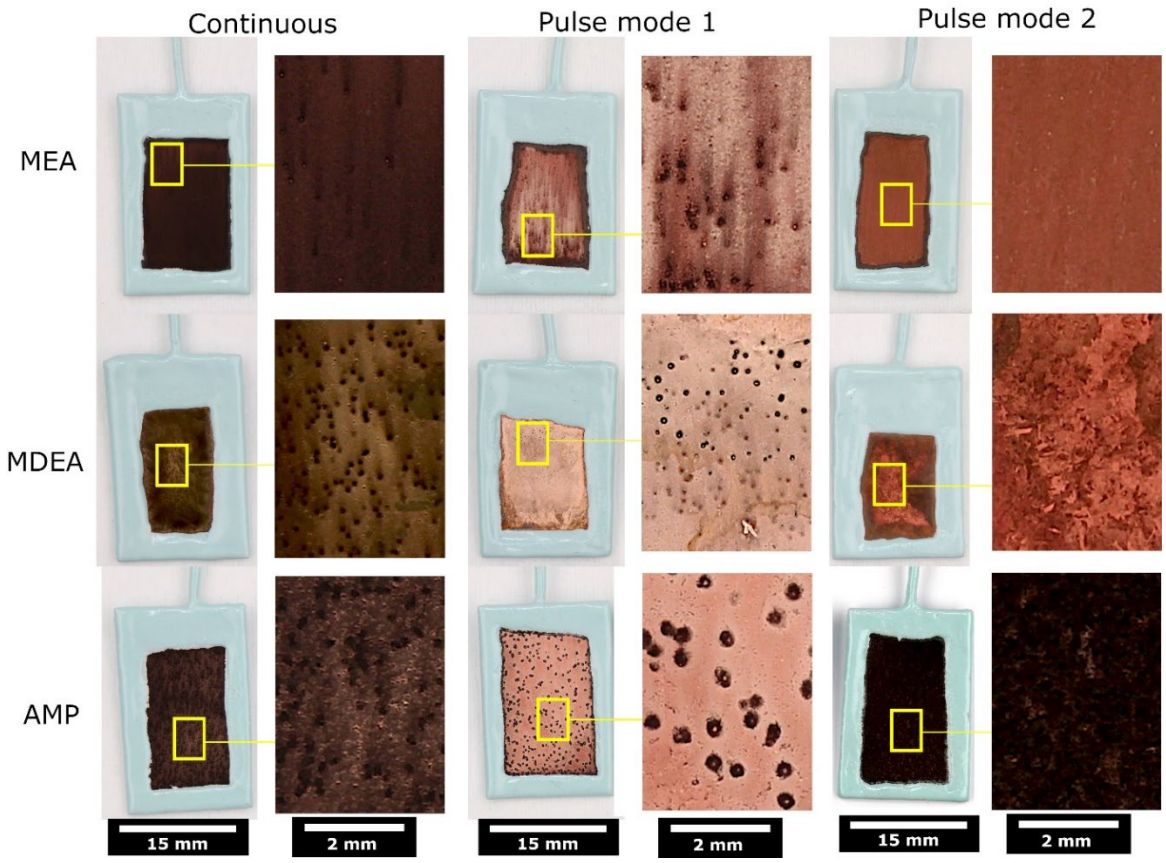

Figure 6. Optical macrographs of catalysts after chronopotentiometry.

Artefacts resulting from gas generation at the catalyst surface, characterized by black spots with occasional dark trails directed upward, are discernible in specimens under continuous and pulse mode 1 polarization. However, these artefacts are absent in samples subjected to pulse mode 2, where no such phenomena are observed.

Higher magnification images of the catalyst surface are provided in **Figure 7**. Prior to chronopotentiometry, as shown in Figure 7a,b, the surface primarily consists of pure copper, characterized by an uneven topology with sporadic overgrown protrusions, ranging from 15 μm to 35 μm in diameter. Post-continuous polarization, the formation of a dark deposit is apparent, leaving only a thin network of exposed copper (Figure 7c,d). Conversely, in MEA under pulse mode 2 (Figure 7e), the surface displays no discernible dark deposits, and the integrity of the surface is notably preserved. An instance of the gas generation artefact, observable in MEA under pulse mode 1 (Figure 7f), exhibits a dark deposit in the shape of a ring, approximately 100 μm in diameter, with a centre of exposed copper corresponding to the cathodic site.

 doi:10.20944/preprints202403.1749.v1

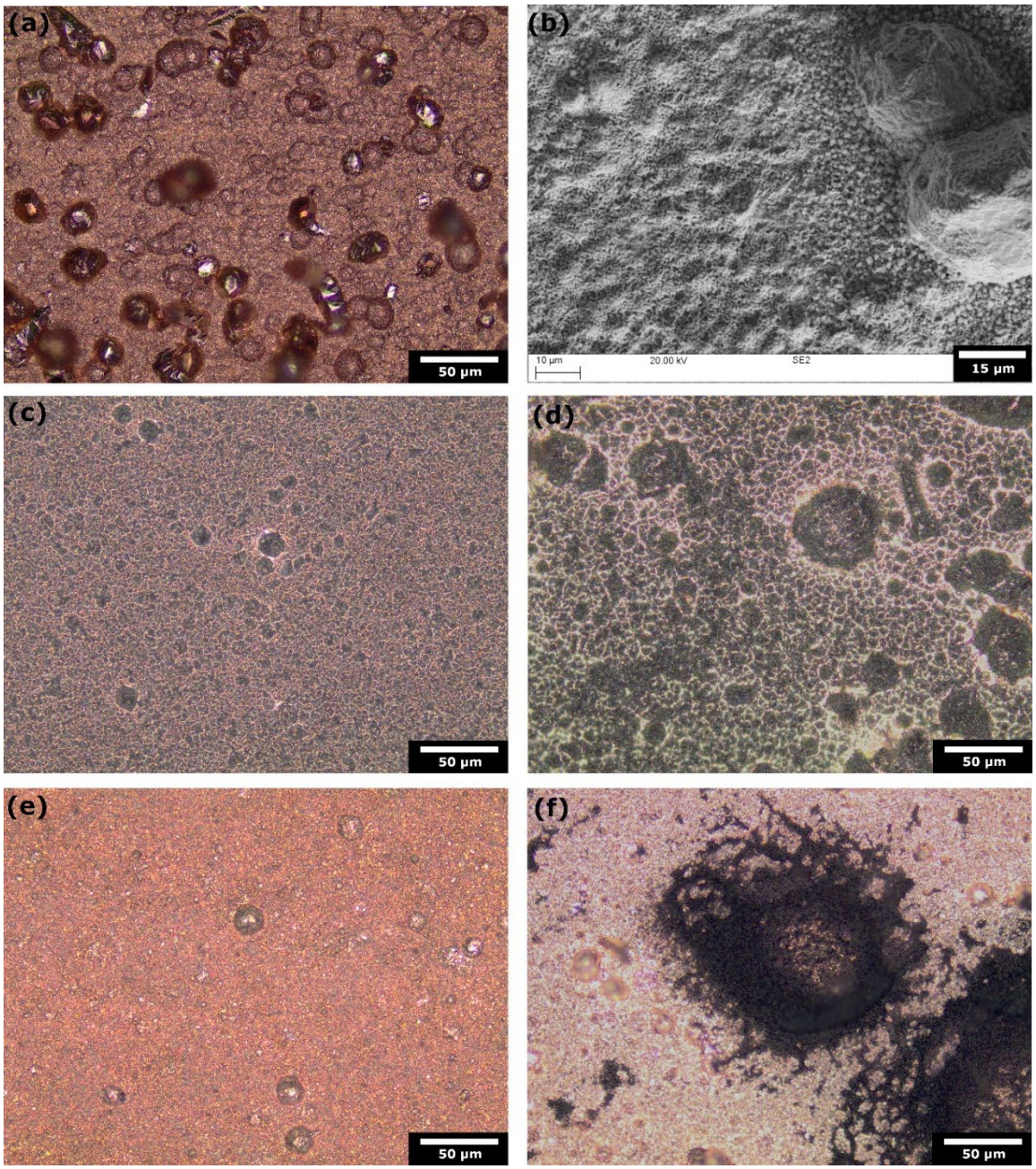

Figure 7. Optical micrographs and SEM of electrodeposited copper catalyst **(a)**, **(b)** prior to chronopotentiometry; **(c)**, **(d)** after continuous chronopotentiometry in MEA and AMP, respectively; **(e)** after pulse mode 2 in MEA; **(f)** after pulse mode 1 in AMP.

4. Discussion

4.1. Corrosion of Copper Catalyst in Amine Media

Corrosion rates were calculated from the corrosion current density (j_{corr}) in accordance with ASTM G102 guidelines [40]. The derived corrosion rates, along with the time necessary to dissolve a 50 µm copper deposit (the estimated thickness based on weight measurements), are tabulated in Table 2. These calculations reveal that the complete dissolution of the copper deposit, under the presumption of exclusive Cu(I) formation and in the absence of any passivation, would necessitate 56 days in the most severe scenario (CO_2-enriched MEA). In the case of Cu(II) formation, the time extends to 112 days. It is critical to recognize that the hypothesis of no passivation is valid only immediately after the termination of cathodic current, as an oxide protective layer is expected to form subsequently. Thus, these calculations are pertinent mainly for approximating the cumulative switch-

 doi:10.20944/preprints202403.1749.v1

off duration tolerable by the catalyst. Accordingly, a cumulative switch-off time threshold of 56 days is considered more than adequate. Therefore, free corrosion of copper in the amine media does not constitute a limiting factor for the catalyst's operational lifespan.

Table 2. Corrosion rates and time required to dissolve a 50 μm thick copper layer, calculated from corrosion current density data in Table 1.

		Dissolution into Cu(I)		Dissolution into Cu(II)	
Media	CO_2	CR / mm y^{-1}	Time / days	CR / mm y^{-1}	Time / days
MEA	no	0.056	328	0.028	655
	yes	0.327	56	0.164	112
MDEA	no	0.007	2623	0.003	5242
	yes	0.023	787	0.012	1573
MDEA/PZ	no	0.009	1967	0.005	3931
	yes	0.021	874	0.010	1747
AMP	no	0.035	525	0.017	1048
	yes	0.179	102	0.089	204
KCl	no	0.056	328	0.028	655

The influence of corrosion-induced surface alterations on the catalyst's efficiency, including aspects such as selectivity, FE, and EE, still requires further investigation. However, existing literature, including findings by [41], indicates that copper oxides favour the reduction of CO_2 into C_{2+} products, suggesting that corrosion may not pose immediate concerns for catalyst functionality.

3.3. Choice of Amine Capture Media for ECR

CO_2 capture in amine media is primarily governed by two processes. The initial process involves the formation of carbamate, as described by reaction (1). Subsequently, the formed carbamate undergoes hydrolysis into bicarbonate, delineated in reaction (2). The prevalence of these reactions is contingent on the amine type. Non-sterically hindered primary amines, such as MEA, tend to form stable carbamate; thus, reaction (1) predominates, leading to almost complete CO_2 capture in the form of carbamate [42]. While this mechanism offers rapid capture kinetics, it necessitates higher energy for CO_2 release.

In sterically hindered amines like AMP, the carbamate bond is less stable [36,43], enhancing the carbamate hydrolysis reaction (reaction 2). This results in CO_2 being stored as both carbamate and bicarbonate, combining the fast capture kinetics of reaction (1) with an increased CO_2 absorption capacity due to the 1:1 stoichiometry between CO_2 and the amine molecule in reaction (2), in contrast to the 2:1 ratio in reaction (1).

$$CO_2 + 2R_1R_2NH \rightleftharpoons R_1R_2N^+H_2 \quad (1)$$

$$R_1R_2N^+H_2 + H_2O \rightleftharpoons R_1R_2NH + HCO_3^- \quad (2)$$

Tertiary amines, such as MDEA, do not form carbamate with CO_2. Instead, they function as catalysts for CO_2 hydration [44], leading to exclusive bicarbonate capture as per reaction (3). This mechanism offers a higher absorption capacity, albeit at a slower capture rate.

$$CO_2 + H_2O + R_1R_2R_3N \rightleftharpoons HCO_3^- + R_1R_2R_3N^+H \quad (3)$$

 doi:10.20944/preprints202403.1749.v1

Historically, capturing CO_2 as bicarbonate has been favourable due to its greater absorption capacity and reduced thermal energy requirement for CO_2 release. The findings presented here indicate that tertiary amine can lead to significant carbonate salt precipitation during ECR, as observed in MDEA and MDEA/PZ. In contrast, primary amine do not facilitate carbonate salt formation, as evidenced in MEA and AMP. Based on these observations, primary amines are emerging as more promising candidates for direct ECR applications. This is confirmed by chronopotentiometry results which showed greater stability for MEA.

3.3. Pulse ECR in Amine Media

Pulse chronopotentiometry findings clearly demonstrate that incorporating short anodic segments counteracts the cathodic shift in potential over time, often resulting in an anodic shift in cathodic potentials. This trend suggests an enhancement in the efficiency of reduction reactions, as evidenced by lower overpotentials needed to maintain the target current density. The formation of copper oxides during anodic segments is likely responsible for this anodic potential shift.

Beyond the advantageous potential shift, pulse ECR exhibits a pronounced ability to preserve the catalyst surface, effectively minimizing the formation of dark deposits. These outcomes highlight the necessity for optimization in pulse ECR to enhance results, such as maximizing potential shifts and reducing deposit formation, as exemplified by pulse mode 2 in MEA. The optimization process varies with the media used, as evidenced by the differences in outcomes for MEA and AMP under pulse mode 2. Key considerations for effective pulse ECR include ensuring adequate oxidation of the copper surface by setting a sufficiently long anodic step duration, counter to the approach seen in AMP under pulse mode 2. Additionally, the cathodic step duration should be short enough to prevent excessive deposit formation at gas generation sites, such as observed in AMP under pulse mode 1, which could be problematic to eliminate during subsequent anodic steps.

Carbonate salt formation arises from localized HO^- ion enrichment near the catalyst surface, a byproduct of the CO_2 reduction reaction (CO_2RR) [20]. Previous studies have suggested that pulse ECR can mitigate carbonate salt formation by curbing HO^- accumulation [21,29]. However, the pulse strategies evaluated were ineffective in preventing carbonate salt precipitation in MDEA-based capture media. This outcome implies that tertiary amines favour carbonate salt formation.

5. Conclusions

The investigation into the stability of electrodeposited copper catalysts for Electrochemical Reduction (ECR) in various amine media offers valuable insights into critical aspects of this process. The study underscores several key findings that advance our understanding and pave the way for future research endeavours:

- Corrosion is not a significant impediment to the catalyst's longevity in amine media. Both computational modelling and experimental data corroborate that the inherent corrosion of copper in these conditions does not critically limit the operational lifespan of the catalyst. This insight alleviates concerns regarding the durability of copper catalysts in practical ECR applications.
- Primary amines, particularly MEA, demonstrate a higher compatibility with ECR processes, characterized by the absence of carbonate salt precipitation and more stable potentials over time. This observation emphasizes the importance of considering the amine type in optimizing ECR performance and underscores the potential for tailored catalyst-amine combinations to improve efficiency.
- Pulse ECR demonstrated significant potential in improving ECR stability, manifested by a shift in cathodic potential and effective mitigation of deposit on the catalyst surface through periodic oxidation. This highlights the importance of exploring innovative operational strategies to augment the stability and efficiency of ECR processes.

Future investigations should prioritize delineating the specific products formed from the reduction of amine-carbamate adducts using electrodeposited copper catalysts. Understanding these reaction pathways is paramount for optimizing the ECR processes and expanding their industrial

 doi:10.20944/preprints202403.1749.v1

applications. Additionally, the effect of pulse strategies on ECR productivity needs exploration, particularly in understanding how the intermittent nature of these strategies influences the rate and efficiency of CO_2 conversion.

Supplementary Materials: The following supporting information can be downloaded at the website of this paper posted on Preprints.org, Figure S1: Potentiodynamic polarization of copper specimens in the different amine-based capture media. **(a)** MEA, **(b)** MDEA, **(c)** MDEA/PZ, **(d)** AMP. Scan rate 10 mV min^{-1}.; Figure S2: Linear polarization resistance of copper specimens in the different amine-based capture media. **(a)** MEA, **(b)** MDEA, **(c)** MDEA/PZ, **(d)** AMP. Scan rate 0.125 mV s^{-1}; Table S1: Average cell resistances in the different amine solutions.

Author Contributions: Conceptualization, CP, KKM, and SP; methodology, CP, and KKM; validation, CP; formal analysis, CP.; investigation, CP, and KKM; resources, SP; data curation, CP; writing—original draft preparation, CP, and KKM; writing—review and editing, CP, KKM, and SP; visualization, CP; supervision, KKM, and SP; project administration, SP; funding acquisition, SP. All authors have read and agreed to the published version of the manuscript.

Funding: This research has received funding from the European Union's Horizon 2020 research and innovation program under the Marie Sklodowska-Curie grant agreement No. 885793, and from BEIS under the UK ACT ERA-NET EC GA 691712. November 2021.

Institutional Review Board Statement: Not applicable.

Informed Consent Statement: Not applicable.

Data Availability Statement: Data supporting the work is available in the Supplementary Information file.

Acknowledgments: The authors would like to thank the ACT3 project partners for their contribution and support. The authors would like to thank Dr. Athanasios I. Papadopoulos for his valuable insights.

Conflicts of Interest: Author SP was employed by the company TWI Ltd.. The remaining authors declare that the research was conducted in the absence of any commercial or financial relationships that could be construed as a potential conflict of interest. The funders had no role in the design of the study; in the collection, analyses, or interpretation of data; in the writing of the manuscript; or in the decision to publish the results.

References

1. H. L. van Soest, M. G. J. den Elzen, and D. P. van Vuuren, "Net-zero emission targets for major emitting countries consistent with the Paris Agreement," *Nat Commun*, vol. 12, no. 1, p. 2140, 2021, doi: 10.1038/s41467-021-22294-x.
2. G. T. Rochelle, "Amine Scrubbing for CO2 Capture," *Science (1979)*, vol. 325, no. 5948, pp. 1652–1654, 2009, doi: 10.1126/science.1176731.
3. M. E. Boot-Handford *et al.*, "Carbon capture and storage update," *Energy Environ Sci*, vol. 7, no. 1, pp. 130–189, 2014, doi: 10.1039/C3EE42350F.
4. J. B. Jakobsen, M. H. Rønne, K. Daasbjerg, and T. Skrydstrup, "Are Amines the Holy Grail for Facilitating CO2 Reduction?," *Angewandte Chemie International Edition*, vol. 60, no. 17, pp. 9174–9179, 2021, doi: https://doi.org/10.1002/anie.202014255.
5. I. Sullivan *et al.*, "Coupling electrochemical CO2 conversion with CO2 capture," *Nat Catal*, vol. 4, no. 11, pp. 952–958, 2021, doi: 10.1038/s41929-021-00699-7.
6. D. Wakerley *et al.*, "Gas diffusion electrodes, reactor designs and key metrics of low-temperature CO2 electrolysers," *Nat Energy*, vol. 7, no. 2, pp. 130–143, 2022, doi: 10.1038/s41560-021-00973-9.
7. S. Nitopi *et al.*, "Progress and Perspectives of Electrochemical CO2 Reduction on Copper in Aqueous Electrolyte," *Chem Rev*, vol. 119, no. 12, pp. 7610–7672, Jun. 2019, doi: 10.1021/acs.chemrev.8b00705.
8. M. G. Kibria *et al.*, "Electrochemical CO2 Reduction into Chemical Feedstocks: From Mechanistic Electrocatalysis Models to System Design," *Advanced Materials*, vol. 31, no. 31, 2019, doi: 10.1002/adma.201807166.
9. F. P. García de Arquer *et al.*, "CO2 electrolysis to multicarbon products at activities greater than 1 A cm−2," *Science (1979)*, vol. 367, no. 6478, pp. 661–666, 2020, doi: 10.1126/science.aay4217.
10. Y. Wang, J. Liu, and G. Zheng, "Designing Copper-Based Catalysts for Efficient Carbon Dioxide Electroreduction," *Advanced Materials*, vol. 33, no. 46, p. 2005798, 2021, doi: https://doi.org/10.1002/adma.202005798.
11. C. Xiao and J. Zhang, "Architectural Design for Enhanced C2 Product Selectivity in Electrochemical CO2 Reduction Using Cu-Based Catalysts: A Review," *ACS Nano*, vol. 15, no. 5, pp. 7975–8000, 2021, doi: 10.1021/acsnano.0c10697.

12. J. Zhao, S. Xue, J. Barber, Y. Zhou, J. Meng, and X. Ke, "An overview of Cu-based heterogeneous electrocatalysts for CO2 reduction," *J Mater Chem A Mater*, vol. 8, no. 9, pp. 4700–4734, 2020, doi: 10.1039/C9TA11778D.
13. S. Popović, M. Smiljanić, P. Jovanovič, J. Vavra, R. Buonsanti, and N. Hodnik, "Stability and Degradation Mechanisms of Copper-Based Catalysts for Electrochemical CO2 Reduction," *Angewandte Chemie International Edition*, vol. 59, no. 35, pp. 14736–14746, 2020, doi: https://doi.org/10.1002/anie.202000617.
14. J. Huang *et al.*, "Potential-induced nanoclustering of metallic catalysts during electrochemical CO2 reduction," *Nat Commun*, vol. 9, no. 1, 2018, doi: 10.1038/s41467-018-05544-3.
15. G. H. Simon, C. S. Kley, and B. Roldan Cuenya, "Potential-Dependent Morphology of Copper Catalysts During CO2 Electroreduction Revealed by In Situ Atomic Force Microscopy," *Angewandte Chemie International Edition*, vol. 60, no. 5, pp. 2561–2568, 2021, doi: https://doi.org/10.1002/anie.202010449.
16. D. Gao, R. M. Arán-Ais, H. S. Jeon, and B. Roldan Cuenya, "Rational catalyst and electrolyte design for CO2 electroreduction towards multicarbon products," *Nat Catal*, vol. 2, no. 3, pp. 198–210, 2019, doi: 10.1038/s41929-019-0235-5.
17. P. Grosse, D. Gao, F. Scholten, I. Sinev, H. Mistry, and B. Roldan Cuenya, "Dynamic Changes in the Structure, Chemical State and Catalytic Selectivity of Cu Nanocubes during CO2 Electroreduction: Size and Support Effects," *Angewandte Chemie International Edition*, vol. 57, no. 21, pp. 6192–6197, 2018, doi: https://doi.org/10.1002/anie.201802083.
18. H. Jung *et al.*, "Electrochemical Fragmentation of Cu2O Nanoparticles Enhancing Selective C–C Coupling from CO2 Reduction Reaction," *J Am Chem Soc*, vol. 141, no. 11, pp. 4624–4633, 2019, doi: 10.1021/jacs.8b11237.
19. S. Popovic, M. Bele, and N. Hodnik, "Reconstruction of Copper Nanoparticles at Electrochemical CO2 Reduction Reaction Conditions Occurs via Two-step Dissolution/Redeposition Mechanism," *ChemElectroChem*, vol. 8, no. 14, pp. 2634–2639, 2021, doi: https://doi.org/10.1002/celc.202100387.
20. S. Garg *et al.*, "How alkali cations affect salt precipitation and CO2 electrolysis performance in membrane electrode assembly electrolyzers," *Energy Environ Sci*, vol. 16, no. 4, pp. 1631–1643, 2023, doi: 10.1039/D2EE03725D.
21. Y. Xu *et al.*, "Self-Cleaning CO2 Reduction Systems: Unsteady Electrochemical Forcing Enables Stability," *ACS Energy Lett*, vol. 6, no. 2, pp. 809–815, 2021, doi: 10.1021/acsenergylett.0c02401.
22. M. Sassenburg, M. Kelly, S. Subramanian, W. A. Smith, and T. Burdyny, "Zero-Gap Electrochemical CO2 Reduction Cells: Challenges and Operational Strategies for Prevention of Salt Precipitation," *ACS Energy Lett*, vol. 8, no. 1, pp. 321–331, 2023, doi: 10.1021/acsenergylett.2c01885.
23. C. A. Obasanjo, G. Gao, B. N. Khiarak, T. H. Pham, J. Crane, and C.-T. Dinh, "Progress and Perspectives of Pulse Electrolysis for Stable Electrochemical Carbon Dioxide Reduction," *Energy and Fuels*, vol. 37, no. 18, pp. 13601–13623, 2023, doi: 10.1021/acs.energyfuels.3c02152.
24. C. A. Obasanjo *et al.*, "In situ regeneration of copper catalysts for long-term electrochemical CO<inf>2</inf> reduction to multiple carbon products," *J Mater Chem A Mater*, vol. 10, no. 37, pp. 20059–20070, 2022, doi: 10.1039/d2ta02709g.
25. X.-D. Zhang *et al.*, "Asymmetric Low-Frequency Pulsed Strategy Enables Ultralong CO2 Reduction Stability and Controllable Product Selectivity," *J Am Chem Soc*, vol. 145, no. 4, pp. 2195–2206, 2023, doi: 10.1021/jacs.2c09501.
26. H. S. Jeon *et al.*, "Selectivity Control of Cu Nanocrystals in a Gas-Fed Flow Cell through CO2 Pulsed Electroreduction," *J Am Chem Soc*, vol. 143, no. 19, pp. 7578–7587, 2021, doi: 10.1021/jacs.1c03443.
27. T. N. Nguyen *et al.*, "Catalyst Regeneration via Chemical Oxidation Enables Long-Term Electrochemical Carbon Dioxide Reduction," *J Am Chem Soc*, vol. 144, no. 29, pp. 13254–13265, 2022, doi: 10.1021/jacs.2c04081.
28. J. Yano and S. Yamasaki, "Pulse-mode electrochemical reduction of carbon dioxide using copper and copper oxide electrodes for selective ethylene formation," *J Appl Electrochem*, vol. 38, no. 12, pp. 1721–1726, 2008, doi: 10.1007/s10800-008-9622-3.
29. E. R. Cofell *et al.*, "Potential Cycling of Silver Cathodes in an Alkaline CO2 Flow Electrolyzer for Accelerated Stress Testing and Carbonate Inhibition," *ACS Appl Energy Mater*, vol. 5, no. 10, pp. 12013–12021, 2022, doi: 10.1021/acsaem.2c01308.
30. M. Abdinejad, Z. Mirza, X. Zhang, and H.-B. Kraatz, "Enhanced Electrocatalytic Activity of Primary Amines for CO2 Reduction Using Copper Electrodes in Aqueous Solution," *ACS Sustain Chem Eng*, vol. 8, no. 4, pp. 1715–1720, 2020, doi: 10.1021/acssuschemeng.9b06837.
31. B. Bohlen, N. Daems, and T. Breugelmans, "Electrochemical Production of Formate Directly from Amine-Based CO2 Capture Media," *ECS Meeting Abstracts*, vol. MA2023-01, no. 26, p. 1722, 2023, doi: 10.1149/MA2023-01261722mtgabs.
32. M. N. Hossain, S. Ahmad, I. S. da Silva, and H.-B. Kraatz, "Electrochemical Reduction of CO2 at Coinage Metal Nanodendrites in Aqueous Ethanolamine," *Chemistry – A European Journal*, vol. 27, no. 4, pp. 1346–1355, 2021, doi: https://doi.org/10.1002/chem.202003039.

33. L. Chen *et al.*, "Electrochemical Reduction of Carbon Dioxide in a Monoethanolamine Capture Medium," *ChemSusChem*, vol. 10, no. 20, pp. 4109–4118, 2017, doi: https://doi.org/10.1002/cssc.201701075.
34. D. Filotás, T. Nagy, L. Nagy, P. Mizsey, and G. Nagy, "Extended Investigation of Electrochemical CO2 Reduction in Ethanolamine Solutions by SECM," *Electroanalysis*, vol. 30, no. 4, pp. 690–697, 2018, doi: https://doi.org/10.1002/elan.201700693.
35. P. T. Frailie and G. T. Rochelle, "Kinetics of Aqueous Methyldiethanolamine/Piperazine for CO2 Capture," in *Process Systems and Materials for CO2 Capture*, 2017, pp. 137–152. doi: https://doi.org/10.1002/9781119106418.ch5.
36. G. Sartori and D. W. Savage, "Sterically hindered amines for carbon dioxide removal from gases," *Industrial & Engineering Chemistry Fundamentals*, vol. 22, no. 2, pp. 239–249, 1983, doi: 10.1021/i100010a016.
37. K. R. Trethewey and J. Chamberlain, *Corrosion for science and engineering, second edition*. United States: NACE International, Houston, TX (United States), 1995. [Online]. Available: https://www.osti.gov/biblio/378108
38. B. Beverskog and I. Puigdomenech, "Revised Pourbaix Diagrams for Copper at 25 to 300°C," *J Electrochem Soc*, vol. 144, no. 10, p. 3476, 1997, doi: 10.1149/1.1838036.
39. S. M. Abd el Haleem and B. G. Ateya, "Cyclic voltammetry of copper in sodium hydroxide solutions," *J Electroanal Chem Interfacial Electrochem*, vol. 117, no. 2, pp. 309–319, 1981, doi: https://doi.org/10.1016/S0022-0728(81)80091-5.
40. G. Astm, "Standard practice for calculation of corrosion rates and related information from electrochemical measurements," *G102-89, ASTM International, West Conshohocken, USA*, 2004.
41. C. W. Li and M. W. Kanan, "CO2 Reduction at Low Overpotential on Cu Electrodes Resulting from the Reduction of Thick Cu2O Films," *J Am Chem Soc*, vol. 134, no. 17, pp. 7231–7234, 2012, doi: 10.1021/ja3010978.
42. N. MacDowell *et al.*, "An overview of CO2 capture technologies," *Energy Environ Sci*, vol. 3, no. 11, pp. 1645–1669, 2010, doi: 10.1039/C004106H.
43. F. Bougie and M. C. Iliuta, "Sterically Hindered Amine-Based Absorbents for the Removal of CO2 from Gas Streams," *J Chem Eng Data*, vol. 57, no. 3, pp. 635–669, 2012, doi: 10.1021/je200731v.
44. M. Edali, A. Aboudheir, and R. Idem, "Kinetics of carbon dioxide absorption into mixed aqueous solutions of MDEA and MEA using a laminar jet apparatus and a numerically solved 2D absorption rate/kinetics model," *International Journal of Greenhouse Gas Control*, vol. 3, no. 5, pp. 550–560, 2009, doi: https://doi.org/10.1016/j.ijggc.2009.04.006.